Electrochimica Acta 196 (2016) 33–40

Contents lists available at ScienceDirect

Electrochimica Acta

journal homepage: www.elsevier.com/locate/electacta

Nano-particle size effect on the performance of $Li_4Ti_5O_{12}$ spinel

Ali Ghorbani Kashkooli[a], Gregory Lui[a], Siamak Farhad[b,*], Dong Un Lee[a], Kun Feng[a], Aiping Yu[a], Zhongwei Chen[a,*]

[a] Department of Chemical Engineering, University of Waterloo, Waterloo, ON N2L 3G1, Canada
[b] Department of Mechanical Engineering, University of Akron, Akron, OH 44325-3903, United States

ARTICLE INFO

Article history:
Received 6 November 2015
Received in revised form 26 January 2016
Accepted 21 February 2016
Available online 26 February 2016

Keywords:
Lithium titanate
Nano technology
Nano-particle
Experiment-based modeling

ABSTRACT

The effect of nano-scale particle size on the performance of $Li_4Ti_5O_{12}$ (LTO) electrode is investigated by computational simulation. Newman pseudo-2D (P2D) model is utilized to characterize the performance of LTO electrode. However, unlike previous P2D lithium ion battery (LIB) models, the model design adjustable parameters are set based on the experimental data obtained from monodispersed active electrode particles. This allows the model to accurately reflect real battery performance. The model provides the optimum nano-particle size for a specific application, which eliminates the performance loss due to the limited mass transportation. The model can be employed for a wide range of electrode materials to optimize the particle-size and reduce fabrication costs by avoiding unnecessary particle size reduction.

1. Introduction

Motivated by their high energy and power density, continued efforts have been devoted to improving and optimizing the performance of LIBs [1,2]. One practical approach is using nano-particle based electrodes to increase interfacial surface area while decreasing the lithium ion diffusion length within the particles to enhance active material utilization [3–6]. Computer models have been proved to be invaluable for investigating the effects of different materials design parameters, e.g. particle size, on the performance of electrochemical energy storage systems [7–10]. In addition, they can be used to find suitable design parameters needed to achieve the energy and power densities that are highly tailored for specific applications [11,12]. Christensen et al. [13] developed a full-cell LTO-$LiMn_2O_4$ (LMO) model to optimize cell design in terms of thickness, and porosity. They further investigated the effect of particle size on the performance of the LTO-LMO. Stewart et al. [14] developed an asymmetric hybrid supercapacitor model by pairing LTO with an activated carbon electrode and compared the model to experimental results. They used their model to characterize the cell discharge/charge curves and to optimize electrode thickness and porosity in order to meet the requirements of hybrid-electric vehicle applications.

Despite the availability of such computer models, there still exists a gap between the simulated results and actual experimental data when selecting a specific particle size for certain applications. In the modeling community, alongside of model developments, experimental data is also obtained to set the model design adjustable parameters based on the model-experiment comparison [13–15]. Experimental data is usually obtained from the half/full cell performance evaluations of the commercial electrode materials having no distinct particle size. Unfortunately, most materials suppliers provide only the maximum particle size without any details on the particle distribution. Then, modeling experts utilize the average particle size in their models determined by Brunauer–Emmett–Teller experiment (BET) measurements [14,15]. Afterwards, they set the model design adjustable parameters by comparing performance of their models with the commercial material electrode. Finally, the model is employed to investigate the influence of particle size on the cell performance and to determine optimum particle size for a specific application. Even though the models are well-developed based on fundamental physical and electrochemical equations, the results are not reliable to interpret the effect of particle size on the performance.

In the present work, we have successfully developed a model to accurately predict real experimental data, not by changing fundamental equations, but by using model adjustable parameters based on the LIB electrode made from a series of mono-dispersed LTO nano-particles having different particle sizes. LTO is used for the experiment as it is one of the most promising anode materials for LIB [1,4]. LTO based electrodes are known to have very good

* Corresponding authors.
E-mail addresses: sfarhad@uakron.edu (S. Farhad), zhwchen@uwaterloo.ca (Z. Chen).

http://dx.doi.org/10.1016/j.electacta.2016.02.153
0013-4686/

Nomenclature

a	specific interfacial area (m^2/m^3)
c	concentration of electrolyte ($mol\,m^{-3}$)
D	diffusion coefficient ($m^2\,s^{-1}$)
f	mean molar activity coefficient
F	Faraday's constant, 96487 ($C\,mol^{-1}$)
i	current density ($A\,m^{-2}$)
I	total applied current density to the cell ($A\,m^{-2}$)
j_n	pore-solid flux of lithium ions ($mol/(m^3\,.s)$)
k_0	reaction rate constant $\left(molm^{-2}s^{-1}(molm^{-3})^{-1.5}\right)$
l	thickness (m)
R_g	universal gas constant (J/(mol K))
R_p	particle size (radius) (m)
t	time (s)
T	temperature (K)
t_+	transference number of lithium-ion with respect to the solvent
U	Open circuit potential of LTP (V)
x	spatial coordinate along the thickness of the cell

Greek letters

α	apparent transfer coefficient (kinetic parameter)
ε	porosity
κ	electrolyte conductivity ($S\,m^{-1}$)
σ	conductivity of solid matrix ($S\,m^{-1}$)
ϕ	electric potential (V)
τ	electrode tortuosity
η	surface overpotential (V)

Subscripts

1	Solid phase
2	electrolyte phase
a	anodic
c	cathodic
eff	effective
ini	initial
LTO	$Li_4Ti_5O_{12}$
max	maximum
s	solid/electrolyte interface
sep	separator
pos	positive electrode

lithium ion intercalation and de-intercalation reversibility and exhibit no structural change (zero-strain insertion material) [3–5] during charge–discharge cycling. Additionally, LTO offers an interesting option compared to graphite for the anode of LIB. Unlike graphite, LTO operates within the stable voltage window of the electrolyte with reduced solid electrolyte interphase (SEI) formation [6,16]. Therefore, the novel method of data prediction presented in this study will be elaborated through the discussion of the model development using LTO nano-particle based electrode.

2. Experimental

2.1. Synthesis of $Li_4Ti_5O_{12}$

Direct synthesis of monodispersed LTO particles of various sizes is difficult due to methods by which they are synthesized [17–19]. Hydrothermal and solid-state methods often lead to particle agglomeration or sintering, which increases the complexity and reduces the reliability of a model for such a system [20,21]. We have found that simplest and most reliable route for LTO synthesis would be a two-step process: i) synthesis of monodisperse TiO_2 particles of varying size; and ii) solid-state conversion of TiO_2 to LTO particles using carbon as a means of blocking Ti diffusion and suppressing TiO_2 sintering, thereby maintaining individual particle morphology [22].

250 nm LTO nanoparticles were synthesized as outlined in literature [23]. In a typical synthesis, 0.4 mL 0.1 M KCl solution was added to 100 mL ethanol. 2.5 mL titanium butoxide was added to the solution and stirred for 10 minutes. The solution was then aged at ambient temperature for 18 hours to form monodisperse 250 nm TiO_2 nanoparticles. After aging, the nanoparticles was centrifuged and washed several times with de-ionized water and ethanol before drying overnight at 60°C. In order to aid the conversion of TiO_2 to LTO, the TiO_2 nanoparticles were heat treated to 500°C at $1°C\,min^{-1}$. This brief heat treatment was used to form crystalline anatase with a small domain size, which has been shown to reduce the onset conversion temperature to LTO and increase LTO purity [24].

Both carbon-coating and conversion to LTO were achieved in a one-step pyrolysis reaction. TiO_2 nanoparticles were first dispersed in an aqueous solution containing 10 wt% glucose and stirred at 70°C in a sealed container for several hours. After adequate mixing, the solution was dried in an oven at 80°C to form a light brown powder. The nanoparticles were then thoroughly mixed with lithium carbonate in a molar ratio of 1:1.03 and heated to 800°C for 6 h in Ar atmosphere to achieve carbon-coated LTO nanoparticles.

2.2. Characterization

The morphology and crystal structure of all materials were confirmed using field-emission scanning electron microscopy (FESEM, Zeiss ULTRA Plus; 10 kV acceleration voltage), transmission electron microscopy (TEM, JEOL 2010F; 200 kV acceleration voltage), X-ray diffraction (XRD, Bruker AXS D8 Advance), and Raman spectroscopy (Bruker SENTERRA; 532 nm 20 mW laser).

2.3. Cell fabrication

The experimental performance of the LTO nanoparticles was determined by fabricating a coin half-cell. An electrode slurry containing LTO was created using Super-P carbon black as the conductive additive, Polyvinylidene fluoride (PVDF) as the binding agent, and 1-methyl-2 pyrolidinone (NMP) as the solvent. The ratio between LTO, Super-P, and PVDF was 90:5:5. The slurry was then cast on a Cu foil current collector using a doctor blade and dried overnight in a vacuum oven at 100°C. A coin half-cell was fabricated using Li metal as the counter electrode, a Celgard 2500 separator, and a 3:7 *(v/v)* ethylene carbonate and dimethyl carbonate electrolyte solution containing 1 M hexafluorophosphate ($LiPF_6$). Coin cell were assembled in an Ar-filled glove box ($H_2O < 0.5$ ppm, $O_2 < 0.5$ ppm). Charge-discharge measurements were conducted using a NEWARE BTS-5V 10mA battery testing station. All coin cells were cycled at rates ranging from 0.2C to 10C (theoretical capacity C = 175 mAh/g) within a voltage window of 1.0-2.5 V.

3. Modeling and simulation

In this section, the mathematical model employed to study a half-cell LTO device is based on Newman pseudo-2D (P2D) model [11], [25–27]. The P2D model uses porous electrode theory to treat the composite homogenous electrode and concentrated solution theory to describe transport in the solution phase. It is called P2D because the lithium ion transport and electric charge transfer are modeled across the electrode thickness direction, while the diffusion of lithium inside spherical particles is introduced in a

radial pseudo-dimension at each computational node along the thickness direction. Furthermore, the particle size assumed to be unchanged during cell operation. For the transport of lithium ion inside the electrolyte the concentrated solution theory is used, which can be written as:

$$\varepsilon\frac{\partial c_2}{\partial t} = \frac{\partial}{\partial x}\left(D_{eff}\frac{\partial c_2}{\partial x}\right) + aj_n(1-t_+^0) \quad (1)$$

where, $\varepsilon$is the electrode porosity, c_2 is the concentration of lithium ion inside electrolyte, D_{eff} is effective diffusivity, a is the specific surface area which is interfacial surface area per unit volume of electrode, $j_n$is the pore-solid flux of lithium ions, and $t_+^0 t_+^0$ is the transference number of the lithium ion in the solution which is assumed to be constant in this work. The subscripts $i = 1, 2$ are the solid and electrolyte phases, respectively, throughout this paper. The effective diffusivity, D_{eff} of lithium-ion is estimated from the Bruggeman correlation:

$$D_{eff} = D_{LTO}\varepsilon^{1.5} \quad (2)$$

The specific surface area of the electrode, $a$can be estimated from:

$$a = \frac{3(1-\varepsilon)}{R_s}$$

$R_s$is the electrode particle size. Eq. (3) is obtained with the assumption of spherical particle. Furthermore, the accuracy of the estimation is increased for monodispersed particle electrodes.

Electric potential in the solution ϕ_2 is represented by ohm's law as:

$$\frac{\partial\phi_2}{\partial x} = -\frac{i_2}{k_{eff}} + \frac{R_g T}{F}(1-t_+)\left(1+\frac{\partial lnf_2}{\partial lnc_2}\right)\frac{\partial lnc_2}{\partial x} \quad (4)$$

where i_2 is current density in the electrolyte, k_{eff} is effective conductivity, R_g is the universal gas constant, T is temperature, F is Faraday's constant, and f_2 is mean molar activity coefficient of electrolyte and is assumed to be constant. k_{eff} can also be calculated using Bruggeman correlation Eq. (2) by replacing diffusivity, D with electrolyte conductivity, k. This is also valid for all upcoming effective parameters. The electric potential in the solid phase, ϕ_1 is described using ohm's law in solid as follows:

$$I - i_2 = -\sigma_{eff}\frac{\partial\phi_1}{\partial x} \quad (5)$$

where, I is superficial current density, σ_{eff} is effective conductivity of solid matrix.

The lithium ion intercalation reaction in the solid matrix is estimated from the Buter-Volmer equation as:

$$j_n = \frac{I}{F} = \frac{i_0}{F}\left(exp\left(\frac{\alpha_a F}{RT}\eta\right) - exp\left(-\frac{\alpha_c F}{RT}\eta\right)\right) \quad (6)$$

where, η, is the surface overpotential defined as:

$$\eta = U - \phi_1 - \phi_2 \quad (7)$$

and i_0 is the exchange current density defined as:

$$i_0 = Fk_0(c_{2s})^{\alpha}(C_{max} - C_{1s})^{\alpha}C_{1s}{}^{\alpha} \quad (8)$$

where, k_0 is a reaction rate constant, C_{1s} and C_{2s} are the lithium ion concentration at the interface of the active material and electrolyte, respectively, C_{max} is the maximum concentration of lithium ion inside the solid matrix, and U is the open circuit potential which is a function of C_{1s}.

The concentration of lithium ion in the solid phase is determined by Fick's mass transfer equation in spherical coordination:

$$\frac{\partial c_1}{\partial t} = D_{LTO}\left(\frac{\partial^2 c_1}{\partial r^2} + \frac{2}{r}\frac{\partial c_1}{\partial r}\right) \quad (9)$$

Table 1 summarizes the governing equations with corresponding boundary conditions at different regions of half-cell.

4. Results and discussion

The morphology of LTO nano-particles has been confirmed using SEM (Fig. 1). The images show a narrow particle size distribution with a diameter of 250 nm. The crystallinity and phase of the nano-particles have been confirmed using XRD and Raman characterizations. The XRD pattern confirms a pristine spinel phase $Li_4Ti_5O_{12}$ [28]. Raman spectrum typical vibration modes of spinel phase LTO with the addition of characteristic D and G bands that correspond to graphitic carbon which have formed during the second stage of LTO synthesis [29].

Using the model parameters listed in Table 2, simulation result of the model galvanostatic discharge at various rates for a LTO half-cell is obtained and shown in Fig. 2. In addition, Fig. 2 also represents the experimental data of galvanostatic discharge for the coin half-cell fabricated. Model-experimental comparison confirms the model ability to characterize discharge behavior of the LTO half-cell at various rates. The design adjustable parameters including the solid phase diffusion coefficient, D_{LTO}, and solid matrix conductivity, σ, are determined based on the method described in Ref. [15] comparing with the obtained experimental data. It should be noted that the obtained design adjustable parameters corresponds to equally sized active material distribution. This would extend the model capability to be used as a tool to investigate the effect of varying particle sizes on the half-cell performance.

Several particle sizes are examined to study the effect of different nano-particle sizes on the performance of LTO electrode. Fig. 3 shows the galvanostatic discharge performance of LTO electrode with various nano-particle sizes at two different rates of c-rate = 1 and c-rate = 5. At c-rate = 1 for $R_p = 250nm$, the capacity is 166 mAh/g which corresponds to 95 percent of theoretical capacity (LTO theoretical capacity = 175 mAh/g). For $R_p = 100nm$the

Table 1
P2D model governing equations.

Governing Equations	Boundary Conditions
Positive Electrode	
$\varepsilon\frac{\partial c_2}{\partial t} = \frac{\partial}{\partial x}\left(D_{eff}\frac{\partial c_2}{\partial x}\right) + aj_n(1-t_+^0)$	$\frac{\partial c_2}{\partial x}\|_{x=0} = 0$
	$-D_{eff,e}\frac{\partial c}{\partial x}\|_{x=l_e^-} = -D_{eff,s}\frac{\partial c}{\partial x}\|_{x=l_e^+}$
$\frac{\partial\phi_2}{\partial x} = -\frac{i_2}{k_{eff}} + \frac{R_g T}{F}(1-t_+)\left(1+\frac{\partial lnf_2}{\partial lnc_2}\right)\frac{\partial lnc_2}{\partial x}$	$\frac{\partial\phi_2}{\partial x}\|_{x=0} = 0, \phi_2\|_{x=0} = 0$
	$-\kappa_{eff,p}\frac{\partial c}{\partial x}\|_{x=l_e^-} = -\kappa_{eff,s}\frac{\partial c}{\partial x}\|_{x=l_e^+}$
$I - i_2 = -\sigma_{eff}\frac{\partial\phi_1}{\partial x}$	$\frac{\partial\phi_1}{\partial x}\|_{x=0} = -\frac{I}{\sigma_{eff}}$
	$\frac{\partial\phi_1}{\partial x}\|_{x=l_e^-} = 0$
$\frac{\partial c_1}{\partial t} = \frac{1}{r^2}\frac{\partial}{\partial r}\left(r^2 D_1\frac{\partial c_1}{\partial r}\right)$	$\frac{\partial c_1}{\partial x}\|_{r=0} = 0$
	$\frac{\partial c_1}{\partial x}\|_{r=R_i} = -j_n D_1$
$j_n = \frac{I}{F} = \frac{i_0}{F}(exp(\frac{\alpha_a F}{RT}(\phi_1 - \phi_2 - U)) - exp(-\frac{\alpha_c F}{RT}(\phi_1 - \phi_2 - U)))$	
$i_0 = Fk_0(c_{2s})^{\alpha}(C_{max} - C_{1s})^{\alpha}C_{1s}{}^{\alpha}$	
Separator	
$\varepsilon\frac{\partial c_2}{\partial t} = \frac{\partial}{\partial x}\left(D_{eff}\frac{\partial c_2}{\partial x}\right)$	$c\|_{x=l_e^-} = c\|_{x=l_e^+}$
	$\frac{\partial c_2}{\partial x}\|_{x=l_e+l_s} = -\frac{I(1-t_+^0)}{FD}$
$\frac{\partial\phi_2}{\partial x} = -\frac{I}{k_{eff}} + \frac{R_g T}{F}(1-t_+)\left(1+\frac{\partial lnf_2}{\partial lnc_2}\right)\frac{\partial lnc_2}{\partial x}$	$\phi_2\|_{x=l_e^-} = \phi_2\|_{x=l_e^+}$
	$\phi_2\|_{x=l_e+l_s} = 0$
Lithium foil counter electrode	
$j_n = \frac{I}{F} = \frac{i_f}{F}\left(\frac{c_{LTO}}{c_{ini}}\right)\left(exp\left(\frac{\alpha_a F}{RT}\left(\phi_f - \phi_2\right)\right) - exp\left(-\frac{\alpha_c F}{RT}\left(\phi_f - \phi_2\right)\right)\right)$	

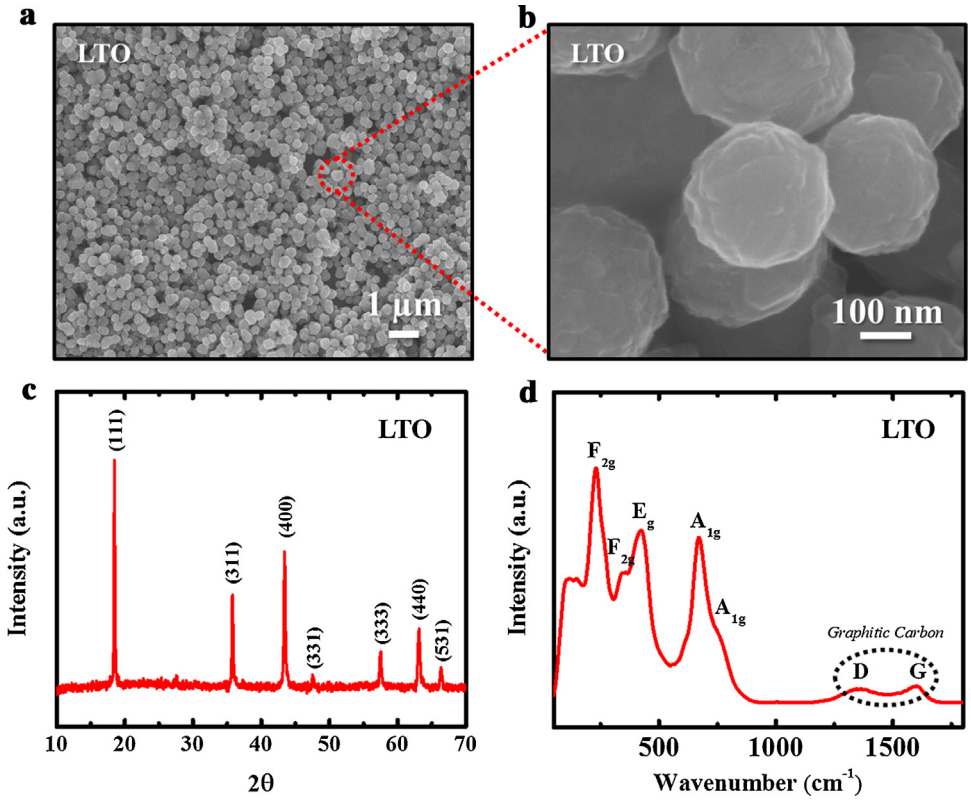

Fig. 1. Characterization of as-synthesized LTO nanoparticles. (a), (b) SEM image of LTO nanoparticles, (c) XRD and (d) Raman spectra of LTO material.

capacity becomes 173 mAh/g which is equivalent to 99 percent of the theoretical capacity, (see Fig. 3a). Further reduction of particle size is unnecessary and causes difficulty in the material synthesis. Fig. 3b demonstrates that at c-rate = 5, for $R_p = 250nm$, the capacity is 130 mAh/g which corresponds to 74 percent of the theoretical capacity. This drop in the active material utilization is a mass transport limit which becomes more prominent as current density increases. Decreasing particle size mitigates lithium ion diffusion path inside the particles and enhance the material rate capability. Fig. 3 shows that at c-rate = 5, decreasing particle size from 250 nm to 50 nm, provides capacity of 173 mAh/g which is equivalent to 99 percent of the theoretical capacity.

In theory, reducing particle size should improve the performance particularly for LTO where the parasitic electrode/electrolyte reactions are absent due to working potential. However, decreasing particle size generally increases the synthesis difficulty and it is wise to design the materials to meet the requirements of a specific application. Hence, there is a trade-off between material utilization and production cost. For instance, in case of the current material, if the maximum practical rate were 5C, nano-particle size of 50 nm would be the best choice since 99 percent of theoretical

Table 2
List of model parameters.

Parameter	Description	Value
A	Area of the electrode	0.9698 cm^2
l_{pos}	Positive electrode thickness	20 μm
l_{sep}	Separator thickness	17 μm
ε_{pos}	Porosity of positive electrode	0.4
ε_{sep}	Porosity of separator	0.55
D_{LTO}	Solid state binary diffusion coefficient of LTO	2.3×10^{-17} m^2/s
σ	Electrical conductivity of positive electrode	0.02 S/m
k_0	Reaction rate constant in positive electrode	$1 \times 10^{-9} molm^{-2}s^{-1}(molm^{-3})^{-1.5}$
α_a	Anodic transfer coefficient	0.5
α_c	Cathodic transfer coefficient	0.5
i_f	Exchange current density of lithium foil	19 A/m^2
c_{ini}	Initial salt concentration in the electrolyte	1000 mol/m^3
c_{max}	Maximum Lithium ion concentration in the LTO particles	22800 mol/m^3
D_{LiPF_6}	Salt diffusivity of electrolyte	7.5×10^{-11} m^2/s
t_+^0	Lithium ion transference number	0.363
T	Cell Temperature	298 K

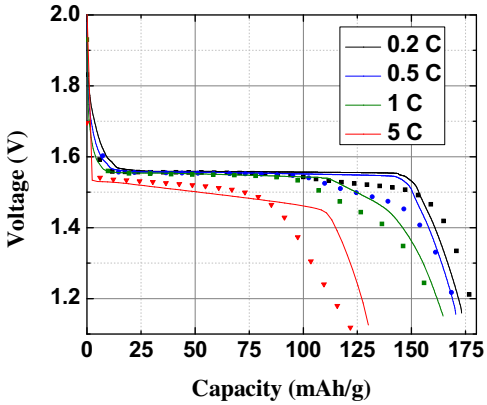

Fig. 2. Comparison of the modeling (line) and experimental (dots) results for a LTO electrode half-cell at different discharge rates.

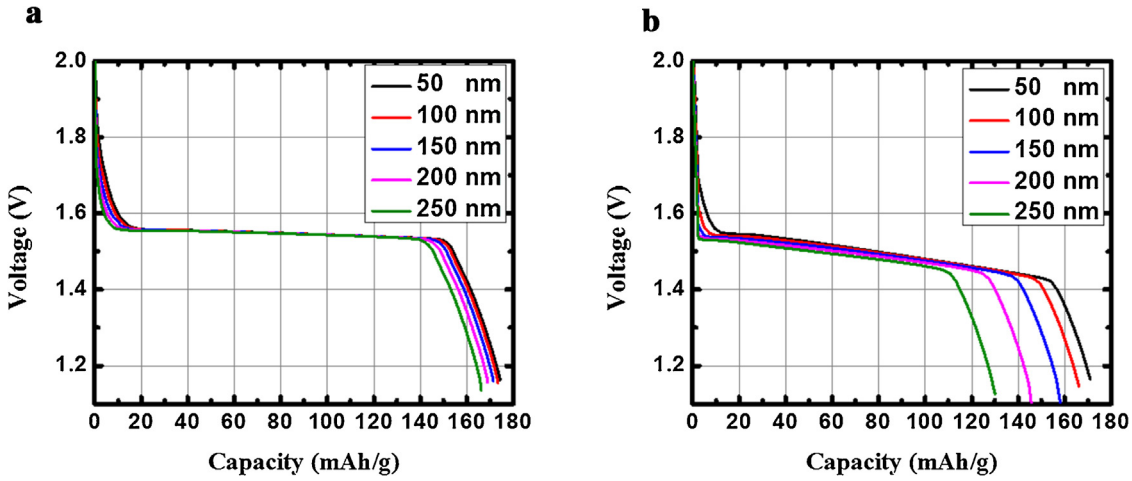

Fig. 3. Galvanostatic discharge performance of LTO electrode with various nano-particle sizes at a) C-rate = 1 b) C-rate = 5.

capacity can be achieved at this rate, see Fig. 3b. In addition, there is no need to reduce particle size further which only increases experimental difficulty. Table 3 summarizes the minimum particle size required at different rates to acquire 99% of the theoretical capacity. It is clear that required particle size should be decreased as discharge rate increases to mitigate lithium ion diffusion length inside the particles.

The drop in active material utilization is be better illustrated by showing the lithium ion concentration distribution inside the LTO nano-particle. The electrochemical reaction of LTO involves a two phase conversion mechanism of lithium-rich and lithium-deficient phases and is commonly described using core-shell model [15]. Based on the core-shell model, there is a single-phase region at the beginning of cell operation. As the reaction proceeds, a two-phase region forms where diffusion of Lithium ion occurs through the shell with the shrinking core of lithium-deficient region. As lithiation continues, the core is totally consumed, and the whole particle will be made of the single Lithium-rich phase. In theory, further lithiation should result in the complete intercalation of the Lithium ion into the active material and fully lithiated particles. However, for large particles, due to long diffusion path of lithium ion, there is not enough time for full lithiation. Fig. 4 represents the lithium ion concentration inside the particle in various locations across the electrode thickness direction at the end of discharge for R_p = 250 nm at c-rate = 5. As mentioned, at the end of discharge the ideal situation of lithium ion concentration inside the LTO particles would be fully lithiated particles across the electrode thickness. However, the observation of a non-uniform lithium ion distribution confirms that there is not enough time for full lithiation due to long diffusion path of lithium ion for a particle with R_p = 250 nm discharged at c-rate = 5. This results in loss of performance due to the lack of material utilization.

Table 3
Minimum particle size required to obtain 99% of theoretical capacity.

Discharge rate	0.2	0.5	1	5
Particle size (nm)	250	150	100	50

The long diffusion path inside the particle at c-rate = 5 can be decreased by employing smaller particle sizes. Fig. 5 represents the lithium ion concentration inside the particle in various locations across the electrode thickness direction at the end of discharge for a particle with R_p = 50 nm. The particles at the current collector location are fully lithiated at the end of discharge. Moreover, in other locations along the electrode thickness, lithium ion

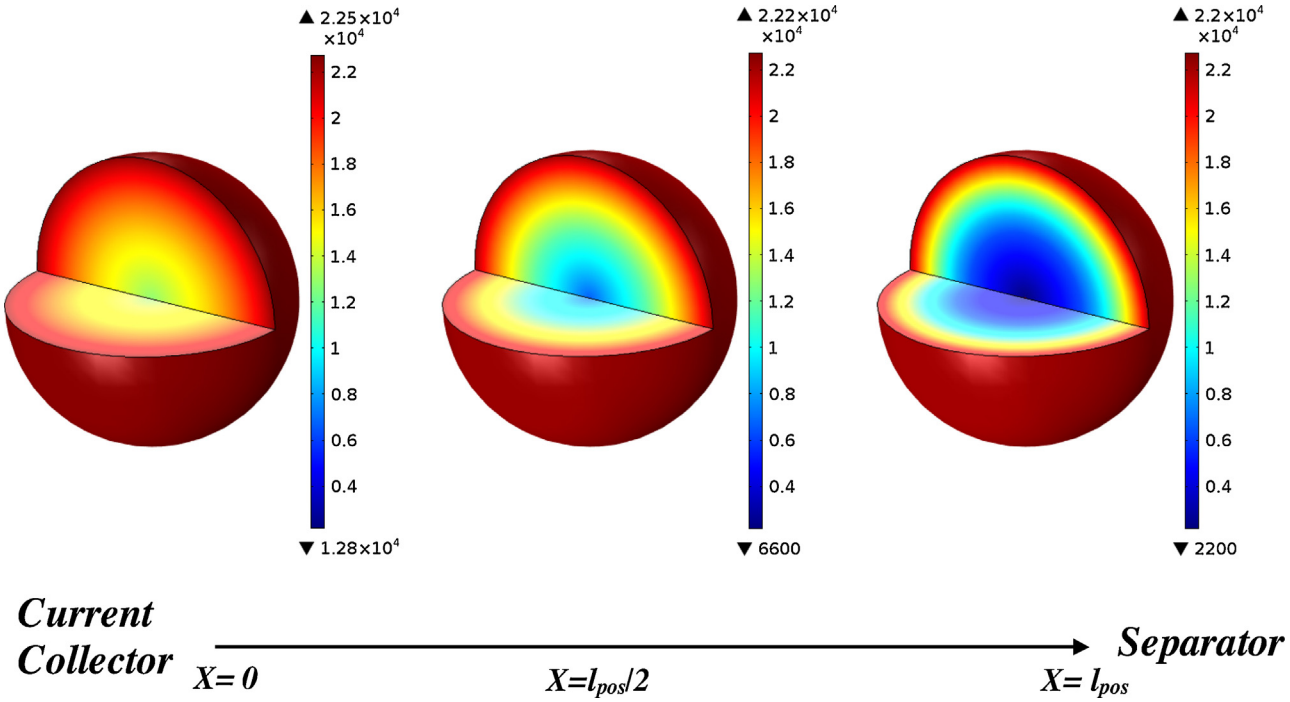

Fig. 4. Distribution of lithium ion concentration (mol/m^3) inside the LTO nano-particle with R_p = 250 nm discharged at c-rate = 5 across the electrode thickness direction at the end of discharge.

concentration is more uniformly distributed compared to the electrode with R_p = 250 nm particles.

In order to quantitatively analyze the local lithium ion concentration variations, histogram graphs are used to show the property distributions based on the discharge simulation results obtained at c-rate = 5. Fig. 6 represents the histogram of lithium ion concentration inside the particle for the size of R_p = 250 nm across the electrode thickness direction at the end of discharge. The ideal condition for the lithium ion concentration as mentioned would be fully lithiated active material with a uniform distribution of $c_{max} = 22800 mol/m^3$. However, Fig. 6 shows that lithium ion concentration at current collector location ranges from 13000 to 22800 mol/m^3, at the half of the positive electrode thickness from 6000 to 22800 mol/m^3, and at the electrode-separator interface

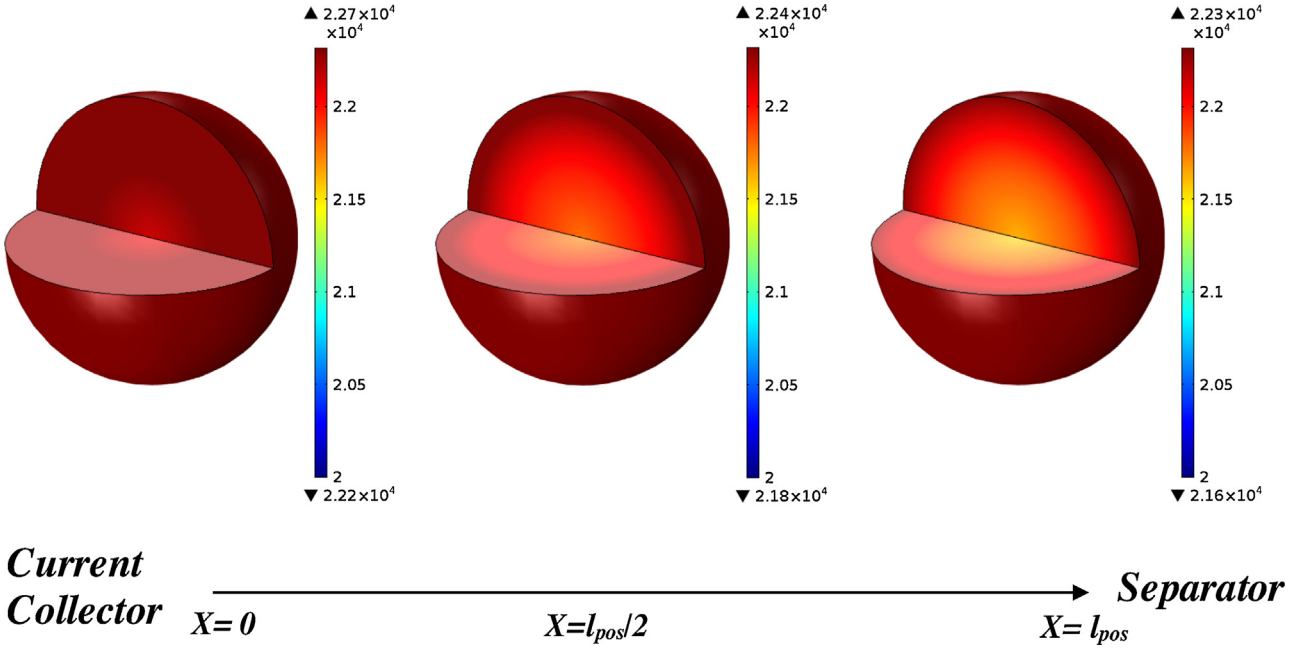

Fig. 5. Distribution of lithium ion concentration (mol/m^3) inside the LTO particle at c-rate = 5 for R_p = 50 nm across the electrode thickness direction at the end of discharge.

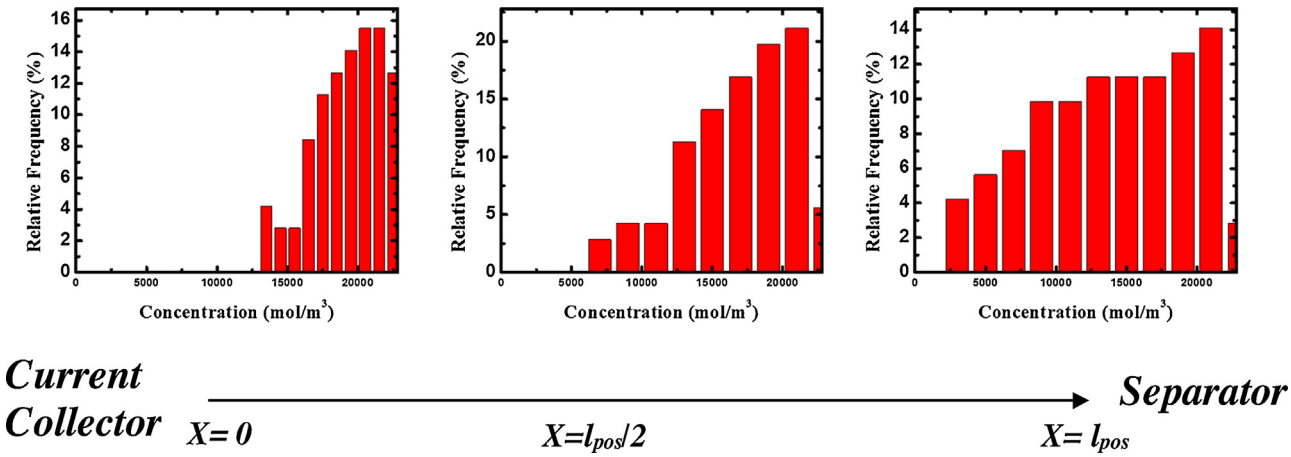

Fig. 6. Histograms of the lithium ion concentration inside particles at c-rate = 5 for a) R_p = 250 nm across the electrode thickness direction at the end of discharge.

from 2500 to 22800 mol/m^3. It is clear that the local concentration range widens moving toward the separator which results in more significant drop in active material utilization.

Fig. 7 shows the lithium ion concentration histogram for particle size of R_p = 50 nm at the same conditions. Reducing particle size results in a uniform distribution of lithium ion inside the active nano-particle. Fig. 7 shows that lithium ion concentration at current collector location ranges from 22100 to 22700 mol/m^3, at the half of the positive electrode thickness from 21700 to 22500 mol/m^3, and at the electrode-separator interface from 21600 to 22400 mol/m^3. Unlike with particle having R_p = 250 nm, reducing particle size to 50 nm significantly improves the active material utilization due to the reduction in the length of the diffusion path.

A computational model has been developed providing the capability of choosing proper nano-particle size for a specific application. Newman pseudo-2D model is utilized to study the performance of LTO electrode. The key point that makes this model practical is setting the model design adjustable parameters based on experimental data obtained from a monodispersed particles having 300 nm diameter. The model provides the optimum particle size for a certain application while keeping the production cost at minimum by preventing unnecessary reduction of particle size. The particle size required to obtain 99% of the theoretical capacity for discharge rates of 0.2, 0.5, 1, and 5 have been found to be 250, 150, 100, and 50 nm, respectively. Further reduction in particle size has negligible improvement in terms of lithium diffusion. Therefore, the model can be employed for a wide range of electrode materials to optimize the particle-size and reduce fabrication costs by avoiding unnecessary particle size reduction.

Acknowledgments

This research was supported by the Natural Sciences and Engineering Research Council of Canada (NSERC) through grants to Z.C. and the University of Waterloo. The research also supported by the University of Akron.

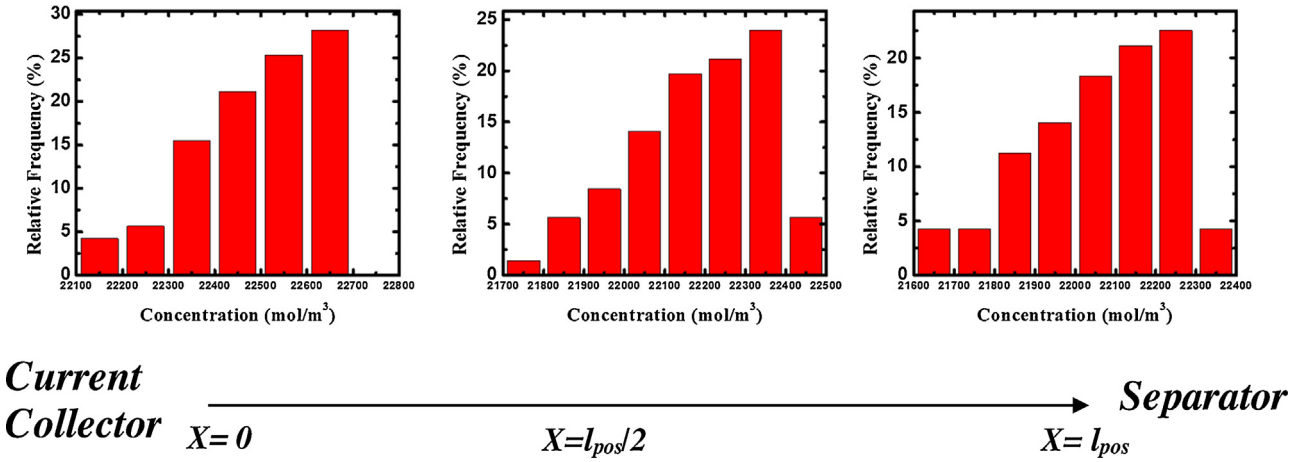

Fig. 7. Histograms of the lithium ion concentration inside particles at c-rate = 5 for a) R_p = 50 nm across the electrode thickness direction at the end of discharge.

References

[1] L. Ruiyi, J. Yuanyuan, Z. Xiaoyan, L. Zaijun, G. Zhiguo, W. Guangli, et al., Significantly enhanced electrochemical performance of lithium titanate anode for lithium ion battery by the hybrid of nitrogen and sulfur co-doped graphene quantum dots, Electrochim. Acta 178 (2015) 303–311, doi:http://dx.doi.org/10.1016/j.electacta.2015.08.018.

[2] D.P. Singh, F.M. Mulder, M. Wagemaker, Templated spinel $Li_4Ti_5O_{12}$ Li-ion battery electrodes combining high rates with high energy density, Electrochem. Commun. 35 (2013) 124–127, doi:http://dx.doi.org/10.1016/j.elecom.2013.08.014.

[3] Y. Qiao, X. Hu, Y. Liu, Y. Huang, $Li_4Ti_5O_{12}$ nanocrystallites for high-rate lithium-ion batteries synthesized by a rapid microwave-assisted solid-state process, Electrochim. Acta 63 (2012) 118–123, doi:http://dx.doi.org/10.1016/j.electacta.2011.12.064.

[4] W. Liu, D. Shao, G. Luo, Q. Gao, G. Yan, J. He, et al., Mesoporous Spinel $Li_4Ti_5O_{12}$ Nanoparticles for High Rate Lithium-ion Battery Anodes, Electrochim. Acta 133 (2014) 578–582, doi:http://dx.doi.org/10.1016/j.electacta.2014.04.072.

[5] Z. Jia, Q. Zhou, X. Li, Y. Fu, H. Ming, J. Zheng, Effect of rigidity of porous structure on electrochemical behavior of pristine $Li_4Ti_5O_{12}$ microspheres, Electrochim. Acta 156 (2015) 216–222, doi:http://dx.doi.org/10.1016/j.electacta.2015.01.017.

[6] C. Xu, L. Xue, W. Zhang, X. Fan, Y. Yan, Q. Li, et al., Hydrothermal Synthesis of $Li_4Ti_5O_{12}/TiO_2$ Nano-composite As High Performance Anode Material for Li-Ion Batteries, Electrochim. Acta 147 (2014) 506–512, doi:http://dx.doi.org/10.1016/j.electacta.2014.09.060.

[7] A. Ghorbani, S. Farhad, V. Chabot, A. Yu, Z. Chen, Effects of structural design on the performance of electrical double layer capacitors, Appl. Energy 138 (2015) 631–639, doi:http://dx.doi.org/10.1016/j.apenergy.2014.09.033.

[8] S. Farhad, F. Hamdullahpur, Optimization of the Microstructure of Porous Composite Cathodes in Solid Oxide Fuel Cells, AIChE J. 58 (2012) 1248–1261, doi:http://dx.doi.org/10.1002/aic.

[9] S. Farhad, F. Hamdullahpur, Micro-Modeling of Porous Composite Anodes for Solid Oxide Fuel Cells, IFAC Proc. 58 (2012) 1893–1906, doi:http://dx.doi.org/10.1002/aic.

[10] A.G. Kashkooli, S. Farhad, A.S. Fung, Z. Chen, Effect of convective mass transfer on lead-acid battery performance, Electrochim. Acta 97 (2013) 278–288, doi:http://dx.doi.org/10.1016/j.electacta.2013.02.116.

[11] M. Doyle, J. Newman, The use of mathematical modeling in the design of lithium/polymer battery systems, Electrochim. Acta 40 (1995) 2191–2196, doi:http://dx.doi.org/10.1016/0013-4686(95) 00162-8.

[12] M. Doyle, Comparison of Modeling Predictions with Experimental Data from Plastic Lithium Ion Cells, J. Electrochem. Soc. 143 (1996) 1890, doi:http://dx.doi.org/10.1149/1.1836921.

[13] J. Christensen, V. Srinivasan, J. Newman, Optimization of Lithium Titanate Electrodes for High-Power Cells, J. Electrochem. Soc. 153 (2006) A560, doi:http://dx.doi.org/10.1149/1.2172535.

[14] S. Stewart, P. Albertus, V. Srinivasan, I. Plitz, N. Pereira, G. Amatucci, et al., Optimizing the Performance of Lithium Titanate Spinel Paired with Activated Carbon or Iron Phosphate, J. Electrochem. Soc. 155 (2008) A253, doi:http://dx.doi.org/10.1149/1.2830552.

[15] V. Srinivasan, J. Newman, Discharge Model for the Lithium Iron-Phosphate Electrode, J. Electrochem. Soc. 151 (2004) A1517, doi:http://dx.doi.org/10.1149/1.1785012.

[16] H. Liu, G. Wen, S. Bi, P. Gao, Enhanced rate performance of nanosized $Li_4Ti_5O_{12}$/graphene composites as anode material by a solid state-assembly method, Electrochim. Acta 171 (2015) 114–120, doi:http://dx.doi.org/10.1016/j.electacta.2015.05.008.

[17] A. Nugroho, S.J. Kim, K.Y. Chung, B.-W. Cho, Y.-W. Lee, J. Kim, Facile synthesis of nanosized $Li_4Ti_5O_{12}$ in supercritical water, Electrochem. Commun. 13 (2011) 650–653, doi:http://dx.doi.org/10.1016/j.elecom.2011.03.037.

[18] K. Kanamura, T. Chiba, K. Dokko, Preparation of $Li_4Ti_5O_{12}$ spherical particles for rechargeable lithium batteries, J. Eur. Ceram. Soc. 26 (2006) 577–581, doi:http://dx.doi.org/10.1016/j.jeurceramsoc.2005.06.014.

[19] S.S. Lee, K.-T. Byun, J.P. Park, S.K. Kim, H.-Y. Kwak, I.-W. Shim, Preparation of $Li_4Ti_5O_{12}$ nanoparticles by a simple sonochemical method, Dalt. Trans. 4182 (2007), doi:http://dx.doi.org/10.1039/b707164g.

[20] J. Lim, E. Choi, V. Mathew, D. Kim, D. Ahn, J. Gim, et al., Enhanced High-Rate Performance of $Li_4Ti_5O_{12}$ Nanoparticles for Rechargeable Li-Ion Batteries, J. Electrochem. Soc. 158 (2011) A275, doi:http://dx.doi.org/10.1149/1.3527983.

[21] D. Wang, X. Wu, Y. Zhang, J. Wang, P. Yan, C. Zhang, et al., The influence of the TiO2 particle size on the properties of $Li_4Ti_5O_{12}$ anode material for lithium-ion battery, Ceram. Int. 40 (2014) 3799–3804, doi:http://dx.doi.org/10.1016/j.ceramint.2013.09.038.

[22] L. Cheng, J. Yan, G.-N. Zhu, J.-Y. Luo, C.-X. Wang, Y.-Y. Xia, General synthesis of carbon-coated nanostructure $Li_4Ti_5O_{12}$ as a high rate electrode material for Li-ion intercalation, J. Mater. Chem. 20 (2010) 595–602, doi:http://dx.doi.org/10.1039/B914604K.

[23] S. Eiden-Assmann, J. Widoniak, G. Maret, Synthesis and Characterization of Hollow and Non-Hollow Monodisperse Colloidal TiO_2 Particles, J. Dispers. Sci. Technol. 25 (2005) 535–545, doi:http://dx.doi.org/10.1081/DIS-200025719.

[24] Y. Shen, M. Søndergaard, M. Christensen, S. Birgisson, B.B. Iversen, Solid State Formation Mechanism of $Li_4Ti_5O_{12}$ from an Anatase TiO_2 Source, Chem. Mater. 26 (2014) 3679–3686.

[25] H. Zarrin, S. Farhad, F. Hamdullahpur, V. Chabot, A. Yu, M. Fowler, et al., Effects of diffusive charge transfer and salt concentration gradient in electrolyte on Li-ion battery energy and power densities, Electrochim. Acta 125 (2014) 117–123, doi:http://dx.doi.org/10.1016/j.electacta.2014.01.022.

[26] J. Newman, W. Tiedemann, Porous-electrode theory with battery applications, AIChE J. 21 (1975) 25–41, doi:http://dx.doi.org/10.1002/aic.690210103.

[27] V. Chabot, S. Farhad, Z. Chen, A.S. Fung, A. Yu, F. Hamdullahpur, Effect of electrode physical and chemical properties on lithium-ion battery performance, Int. J. Energy Res. 31 (2007) 135–147, doi:http://dx.doi.org/10.1002/er.

[28] J. Li, Z. Tang, Z. Zhang, Controllable formation and electrochemical properties of one-dimensional nanostructured spinel $Li_4Ti_5O_{12}$, Electrochem. Commun. 7 (2005) 894–899, doi:http://dx.doi.org/10.1016/j.elecom.2005.06.012.

[29] H.-K. Kim, J. Jegal, J.-Y. Kim, S. Yoon, K.C. Roh, K. Kim, In situ fabrication of lithium titanium oxide by microwave-assisted alkalization for high-rate lithium-ion batteries, J. Mater. Chem. A 1 (2013) 14849–14852, doi:http://dx.doi.org/10.1039/c3ta13206d.